2D-doped silicon detectors for UV/optical/NIR and x-ray astronomy

Conference or Workshop Item

PROCEEDINGS OF SPIE

SPIEDigitalLibrary.org/conference-proceedings-of-spie

2D-doped silicon detectors for UV/optical/NIR and x-ray astronomy

Michael Hoenk, April Jewell, Gillian Kyne, John Hennessy, Todd Jones, et al.

Michael E. Hoenk, April D. Jewell, Gillian Kyne, John Hennessy, Todd Jones, Samuel Cheng, Shouleh Nikzad, David Morris, Katherine Lawrie, Jesper Skottfelt, "2D-doped silicon detectors for UV/optical/NIR and x-ray astronomy," Proc. SPIE 12191, X-Ray, Optical, and Infrared Detectors for Astronomy X, 1219113 (29 August 2022); doi: 10.1117/12.2631542

SPIE.

Event: SPIE Astronomical Telescopes + Instrumentation, 2022, Montréal, Québec, Canada

2D-doped silicon detectors for UV/optical/NIR and X-ray astronomy

Michael E. Hoenk*[a], April D. Jewell[a], Gillian Kyne[a], John Hennessy[a], Todd Jones[a], Samuel Cheng[a], Shouleh Nikzad [a], David Morris [b], Katherine Lawrie [b], Jesper Skottfelt [c]

[a] Jet Propulsion Laboratory, California Institute of Technology, Pasadena, CA, USA;
[b] Teledyne e2v, 106 Waterhouse Ln, Chelmsford CM1 2QU, United Kingdom;
[c] The Open University, Department of Physical Sciences, Milton Keynes, United Kingdom

ABSTRACT

In this paper we review the physics and performance of back-illuminated CCDs. Models of back-illuminated CCDs are used to derive requirements for stable, strong surface passivation in space-relevant environments. Models and data are used to compare state-of-the-art surface passivation methods with 2D-doped surfaces. MBE growth of 2D-doped silicon on back-illuminated CCDs and CMOS image sensors enables near 100% charge collection efficiency with exceptional stability in space and other harsh environments. Lifetime tests performed on 2D-doped CMOS image sensors using pulsed DUV lasers have demonstrated the unique stability of 2D-doped detectors against high levels of radiation-induced surface damage. The insensitivity of 2D-doped detectors to Si-SiO_2 traps has facilitated the development of a variety of coatings and filters with science-enabling capabilities for NASA instruments and missions in the far and near ultraviolet spectral range. We discuss the status and goals of a strategic partnership between JPL and Teledyne e2v for the certification of 2D-doping processes, and report initial results from our collaboration.

Keywords: UV detectors, delta-doped, silicon, charge coupled device, CMOS Imaging Sensor, Surface passivation, backside charging, ion implantation, delta-doped CCDs, 2D-doped CCDs, X-ray, UV, ultraviolet

1. INTRODUCTION

The recent Astro2020 decadal survey, *Pathways to Discovery in Astronomy and Astrophysics for the 2020s*, identified time domain astronomy and astrophysics as key scientific challenges for the next decade [1]. Highlighting NASA's Transiting Exoplanet Survey Satellite (TESS) Explorer mission for having ushered in a new era of exoplanet physics and time domain astrophysics, the decadal survey emphasizes the importance of ultra-precise optical photometry (light curves), and recommends that NASA establish a time-domain program of small to medium scale missions, including SmallSats, CubeSats, and Explorer missions. The 2D-doped detector technologies described in this paper enable the stability and sensitivity required by these missions over a wide spectral range, spanning soft X-rays through the Ultraviolet (UV), visible, and near infrared. The unique capabilities of 2D-doped detectors will be particularly important in the advancement of silicon detectors to address technology gaps identified in the Astro2020 decadal survey.

Since the invention of charge-coupled devices (CCDs), astronomers have worked to develop and optimize CCDs for spaceborne telescopes. As early as 1974, researchers at Texas Instruments sought to extend the response of CCDs beyond the visible by thinning and back illumination. One of the more challenging obstacles to realizing the potential of CCDs for astronomy has been the passivation of defects and traps at surfaces and interfaces. A long-standing goal has been the achievement of stable, 100% charge collection efficiency in relevant environments for space. In this paper, we review the history of back-illuminated CCDs, develop models of thinned CCD performance, and apply these models to derive requirements for strong surface passivation and stable, high efficiency response in space-relevant thermal and radiation environments. We then apply these requirements to compare surface passivation technologies, and review 2D-doped detector performance in light of data and models. Finally, we discuss the flight heritage of 2D-doped detectors, including our partnership with Teledyne e2v (Te2v) on process qualification and manufacture of 2D-doped detectors for spaceflight.

* Corresponding author: michael.e.hoenk@jpl.nasa.gov; phone 1-818-354-1881; jpl.nasa.gov

X-Ray, Optical, and Infrared Detectors for Astronomy X, edited by Andrew D. Holland, James Beletic
Proc. of SPIE Vol. 12191, 1219113 · © 2022 SPIE · 0277-786X · doi: 10.1117/12.2631542

2. THE HISTORY AND PHYSICS OF THINNED CCDS FOR ASTRONOMY

2.1 Quantum efficiency hysteresis in back-illuminated CCDs

JPL's invention and subsequent development of 2D-doped silicon detectors began with the unexpected discovery of instabilities in CCDs developed for the Hubble Space Telescope Wide Field/Planetary Camera (HST WF/PC). This problem wasn't new, as quantum efficiency hysteresis (QEH) had plagued back-illuminated CCDs from the beginning. Researchers at Texas Instruments (TI) demonstrated the first back-thinned CCDs in 1974 [2]. By doping the back surface to $10^{18}cm^{-3}$ and depositing an antireflection coating, they achieved >50% QE in the 500-900nm spectral range with a 90% peak QE. The UV QE was very low in these early CCDs due to limitations in thinning and passivation, compounded by extremely shallow absorption of UV photons in the CCD surface. This problem was addressed by depositing coronene on the surface of back-illuminated CCDs to convert UV to visible photons that penetrate much deeper in the CCD [3].

In 1984, during system-level thermal vacuum testing of the WF/PC instrument, the coronene-coated CCDs developed severe instabilities caused by defects in the CCD surface [4-6]. These defects trapped positive charge at the Si-SiO_2 interface and depleted the surface, leading to low QE as some photogenerated charge was trapped in the backside potential well. When the CCD was illuminated, electrons partially filled the backside well, temporarily improving QE and leading to the instability known as QEH [7]. To address this problem, the WF/PC camera was retrofitted with a light pipe to periodically flood the CCDs with solar UV radiation, which helped stabilize the response by creating negative charge on the CCD surface. In practice, the UV flood was neither reliable nor permanent in space-relevant environments. The WF/PC CCDs would require periodic recharging on orbit [6].

2.2 Surface accumulation and QE-pinning

The two main approaches to surface passivation, first explored in the 1970's and 1980's, are backside charging and surface doping. Both methods are based on forming a strong electric field near the surface in order to drive photogenerated electrons toward the front surface collection wells, and thereby prevent losses due to recombination at the Si-SiO_2 interface. Backside charging methods passivate the surface with an external electric field, while surface doping methods produce fields internally by creating a doping profile with a high surface density and shallow distribution. Backside charging methods enable the highest possible QE, but they're sensitive to charged defects at the Si-SiO_2 interface. Surface doping methods are relatively insensitive to interface traps, but have lower QE due to recombination in the highly doped surface.

In 1985, Jim Janesick and his collaborators published a seminal paper on the physics of backside charging as a solution to the QEH problem in thinned CCDs [8]. Beginning with models of accumulated silicon surfaces developed for metal-oxide-semiconductor (MOS) transistors, Janesick's team studied the physics of thinned CCDs and derived requirements for achieving a "QE-pinned" state, which they defined as stable, 100% internal quantum efficiency and the associated elimination of QEH. Based on their model, Janesick *et al.* developed the concept of a critical electric field for QE-pinning. According to this theory, photoelectrons generated beyond a critical absorption distance are unable to reach the surface and are therefore detected with high efficiency:

$$X_C = D_n/(\mu|E_s|) \quad (1)$$

To achieve QE-pinning using backside charging, the surface electric field must be strong enough that critical distance is less than the photon absorption length, $\alpha X_C << 1$. At $\lambda = 270\ nm$ (where the photon absorption length is at its minimum), Janesick *et al*. determined that QE-pinning requires an electric field $|Es| >> 5x10^4\ V/cm$, and, after accounting for the voltage drop across the oxide, backside charge densities in excess of 10^{13} e/cm^2.

In 1989, Janesick *et al.* published a follow-on paper in which they described new developments in QE-pinning technologies [10]. By that time, QE-pinning had been demonstrated using backside-charging and flash gate technologies on CCDs from multiple manufacturers. Surface electric fields were reported greater than $2x10^5\ V/cm$ for some types of CCD, which was sufficient for QE-pinning. Chemisorption charging methods are an evolution of the flash gate methods, in which a charged metal layer is embedded in the surface oxide to improve long-term stability of the charged surface [10, 11].

Despite significant progress, a permanent solution to the QEH problem remained elusive. Backside charging and flash gate technologies could not maintain QE-pinning in all relevant environments, including in particular the thermal and vacuum environments relevant to space. In 1993, NASA installed a new WF/PC II instrument on HST. The iconic images from HST were captured by front-illuminated CCDs coated with Lumogen in order to achieve the required UV sensitivity and stability. The search for a stable back-illuminated CCD required a new approach.

2.3 QE(T) in weakly passivated detectors

In their 1989 paper on CCD pinning technologies, Janesick *et al.* reported degradation of QE in an ion-implanted CCD at low temperatures. This detector was nearly QE-pinned at room temperature, but as the CCD was cooled to -120°C the QE decreased significantly [9]. This loss of efficiency was not confined to the UV region of the spectrum, where absorption occurs very close to the surface, but affected the QE over the entire visible/NIR spectral range (400-1000nm). According to Lesser and Iyer, this degradation of QE with temperature is a problem common to all weakly passivated devices [11].

Janesick's 1989 paper doesn't explain the observed degradation of QE with temperature. In that paper, they derived an expression for charge collection efficiency (CCE) by making the heuristic assumption that every electron that interacts with the Si-SiO_2 interface at the CCD back surface will be lost to recombination [9]. Reasoning that half of the photoelectrons generated within the critical distance ($x < X_C$) would be moving toward the back surface and consequently lost to recombination, while the other half would be moving toward the front surface where they would be detected, they derived the following equation for internal quantum efficiency:

$$CCE = 0.5[1 + exp(-\alpha X_C)] \quad (2)$$

where the parameter α is absorption coefficient. As the absorption coefficient depends only weakly on temperature, the only temperature-dependent parameter in this equation is the critical distance. If we apply Einstein's relation, $D/\mu = kT/q$, to equation 1, we find that $X_C = kT/(q|E_s|)$, which suggests that the QE should only degrade with temperature if the surface electric field were to decrease faster than kT as temperature is reduced. That is what happens in a weakly-accumulated CCD, but to understand why we have to look deeper in the detector to see what happens to the silicon conduction band energy at low temperatures.

2.4 Analytical model of QE(T) in thinned CCDs and requirements for stable surface passivation

In order to understand the temperature-dependent QE in weakly passivated detectors, we turn to a simplified model of back-illuminated CCDs developed by Morley Blouke [12]. Blouke's model divides the CCD into three regions: (1) a near-surface barrier with a constant electric field, E_0; (2) a bulk region in which the electric field is zero; and (3) a frontside potential well where photogenerated electrons are collected. This simplified model is amenable to an analytical solution of the current and continuity equations. Blouke justified this simplification by the greater insight it allows into the physics of the problem and the ability to study the influence of individual parameters on detector performance. We will use Blouke's simplified model to assist in our derivation of surface passivation requirements for spaceflight.

With these simplifying assumptions, Blouke solved these equations to calculate the QE of a back-illuminated CCD:

$$E(x) = \begin{cases} E_0 & for\ 0 < x < \sigma \quad Surface\ region \\ 0 & for\ \sigma < x < d \quad Field\ free\ bulk\ silicon \end{cases} \quad (3)$$

$$J(x) = \mu_n n(x) E(x) + D_n \mathrm{dn(x)/dx} \quad (4)$$

$$\delta \mathrm{n}/\delta \mathrm{t} = (1/q)\nabla \cdot J_n(x) + G_n(\mathrm{x}) - R_n \quad (5)$$

$$G_n(x) = \alpha \phi_0 \exp(-\alpha x) \quad (6)$$

$$R_n(x) = \delta n(x)/\tau \quad (7)$$

where α is the wavelength dependent absorption coefficient, ϕ_0 is the photon flux, τ is the recombination lifetime, μ_n is the mobility, and D_n is the diffusion constant. Based on his analytical solutions to these equations, Blouke was able to calculate *J(x)* and *n(x)* at a given wavelength, and from this he derived the following equation for the quantum efficiency:

$$QE(\lambda) = \frac{1-R(\lambda)}{\phi_0} \left[\int_d^t G_n(x)dx - \left(\frac{1}{q}\right) J_n(d) \right] \quad (8)$$

Blouke's model parameterizes surface recombination in the form of a boundary condition on the current. Excess electrons at the surface, quantified in terms of the surface density $\delta n(0)$, are subject to recombination. The rate of recombination at the surface is quantified as a current, *J(0)*, which is proportional to the excess carrier density. The proportionality constant, S_0, has the units of velocity, and is called the surface recombination velocity. The boundary conditions are (1) continuity of $J(x)$ and $n(x)$ at $x = \sigma$; (2) surface current $J(0)/q = S_0 \cdot \delta n(0)$; and (3) electron density at the edge of the depletion region, $n(d) = 0$.

To complete our model of QE(T), we need to incorporate models of temperature-dependent parameters in these equations. In his 2001 book, *Scientific Charge-Coupled Devices*, Janesick reviewed the theory of accumulation that he first published in 1985, with a few notable additions and refinements [13]. Whereas his 1985 paper focused primarily on the surface electric field as the critical parameter for QE-pinning, in 2001 he states that the surface potential at the Si-SiO_2 interface, V_s, is the variable that will define the strength of the accumulation layer. We can write the expression for the potential barrier in a back-illuminated detector as a function of position and temperature as follows:

$$\Delta V_{barrier}(T) = V_{surface} - V_{bulk}(T) \quad (9)$$

If we make the simplifying assumption that the surface potential is pinned, then variation of the potential barrier with temperature is dominated by the bulk potential. This can be calculated using the following equation for the temperature dependence of the Fermi level in p-type silicon, which was cited by Janesick in his 2001 book on scientific CCDs [13]:

$$V_f(T) = kT/q \cdot ln\,(N_A/n_i(T)) \quad (10)$$

where N_A is the dopant density in the detector epilayer and $n_i(T)$ is the intrinsic carrier concentration in silicon. Additional parameters needed to incorporate detector temperature in Blouke's model of thinned CCDs are as follows [14-16]:

$$n_i(T) = 5.29 \times 10^{19} \left(\frac{T}{300}\right)^{2.54} exp\left(-\frac{6726}{T}\right) \quad (11)$$

$$E_g(T) = 1.1666 - (4.73 \times 10^{-4}) \cdot T^2/(T + 636) \quad (12)$$

$$\mu_n = 1.43 \times 10^9 \cdot T^{-2.42} cm^2/V \cdot s \quad (13)$$

$$D_n = \mu_n kT/q \quad (14)$$

With these modifications, Blouke's model provides a quantitative explanation for the temperature-dependent QE observed by Janesick and Lesser in weakly passivated CCDs. The essential parameters are the surface potential, the surface recombination velocity, and the temperature-dependent Fermi level in the field-free region of the detector (Equation 10). Figure 1 shows the application of this model to the degradation of QE with temperature in weakly passivated detectors. Figure 2 shows the charge collection efficiency (CCE) as a function of temperature and surface potential. When the surface recombination is high (10^6 cm/s in this case), we see that increasing the surface potential from -0.2V to -0.3V stabilizes the detector and approaches the QE-pinned ideal. Figure 3 shows that most of the temperature dependence in this model is captured by the normalized energy barrier, $q\Delta V/kT$.

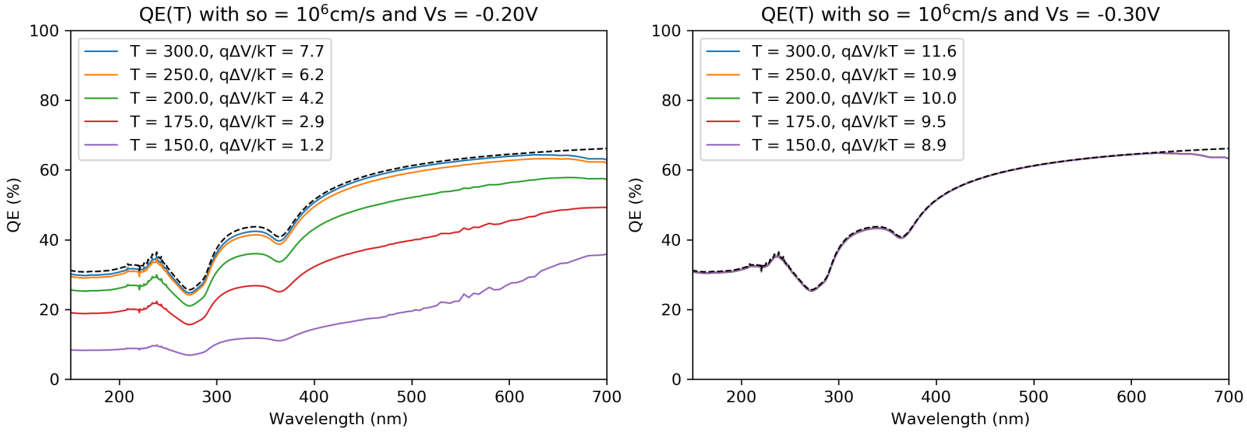

Figure 1: Quantum efficiency degradation with temperature signifies weak surface passivation. This figure shows calculations of QE(*T*) using the temperature-dependent model of thinned CCDs for two different values of the surface potential, *Vs = -0.2V*, and *Vs = -0.3V*. The dashed line represents reflection-limited QE, the ideal response for a QE-pinned detector.

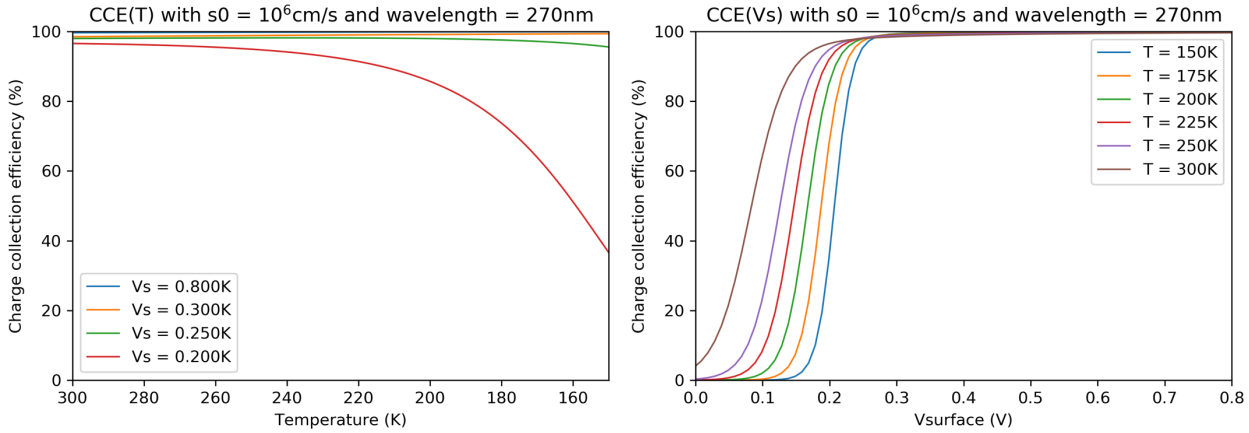

Figure 2: The QE(T) model provides quantitative estimates for the surface passivation strength needed to stabilize a back-illuminated CCD over the full range of operating temperatures for astronomical instruments. This figure shows that a surface potential $Vs > 0.3V$ is required for QE-pinning at all relevant temperatures.

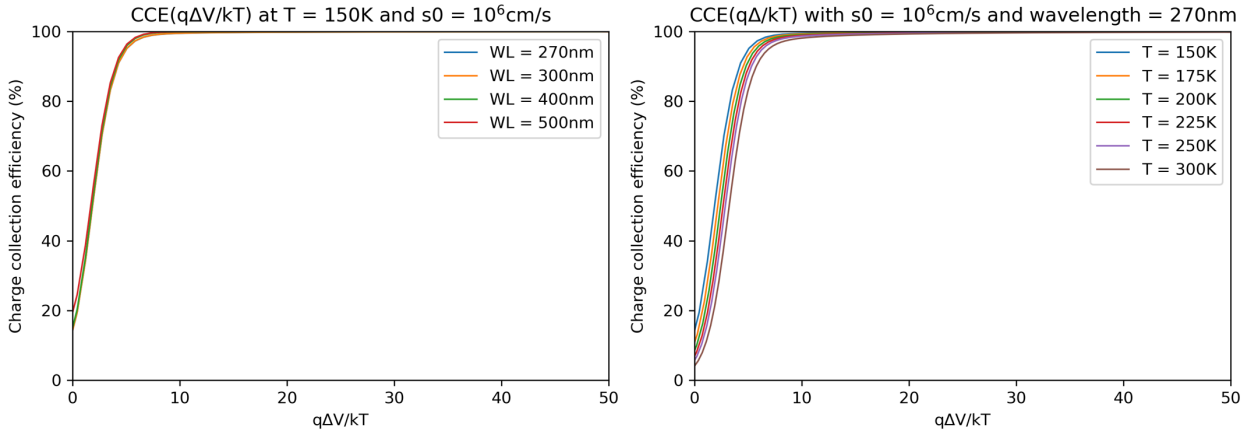

Figure 3: The requirement for stable passivation of back-thinned CCDs can be expressed in terms of the normalized energy barrier, $q\Delta V/kT > 10$. This expression provides a more intuitive explanation for the QE-pinning requirement in terms of energy rather than electric field strength. Comparing this with Figure 2, we see that the normalized energy barrier captures most of the temperature dependence in the QE(T) model of thinned CCDs.

2.5 Degradation of CCD QE and stability caused by ionizing radiation in space-relevant environments

Backside-charging methods, including chemisorption charging and more recently developed methods for growing oxides with fixed negative charge, depend on maintaining a low density of traps near the detector surface [10,11,17]. Janesick *et al.* developed a flash oxide process based on low temperature steam oxidation for the UV flood and flash gate processes [10]. Lesser and Iyer developed a high pressure oxidation process for chemisorption passivation, which achieved interface trap densities less than $2x10^{12}cm^{-2}$ [11]. The dependence of backside charging methods on low interface trap densities carries a risk of failure in high radiation environments. Whereas high quality Si-SiO_2 interfaces can be fabricated with exceptionally low surface trap densities, exposure to ionizing radiation is well known to break bonds in the oxide, thereby increasing the trap density at the Si-SiO_2 interface [18-20]. Back-illuminated detectors are damaged by exposure to high-energy particles and photons in space telescopes and high energy physics experiments, as well as by prolonged exposure to deep and far ultraviolet (DUV and FUV) radiation. Thinned CCDs and CMOS imaging detectors may be QE-pinned in pre-flight tests, and yet suffer severe degradation in space after exposure to ionizing radiation in space.

Whereas ion implantation methods cannot match the high QE achieved with backside charging, highly doped surfaces provide greater stability against time-variable backside charging, QEH and damage from ionizing radiation. For a device passivated by surface doping, radiation-induced traps will increase the surface recombination velocity, but will leave the surface potential relatively unchanged. In contrast, the external electric field produced by backside charging methods are

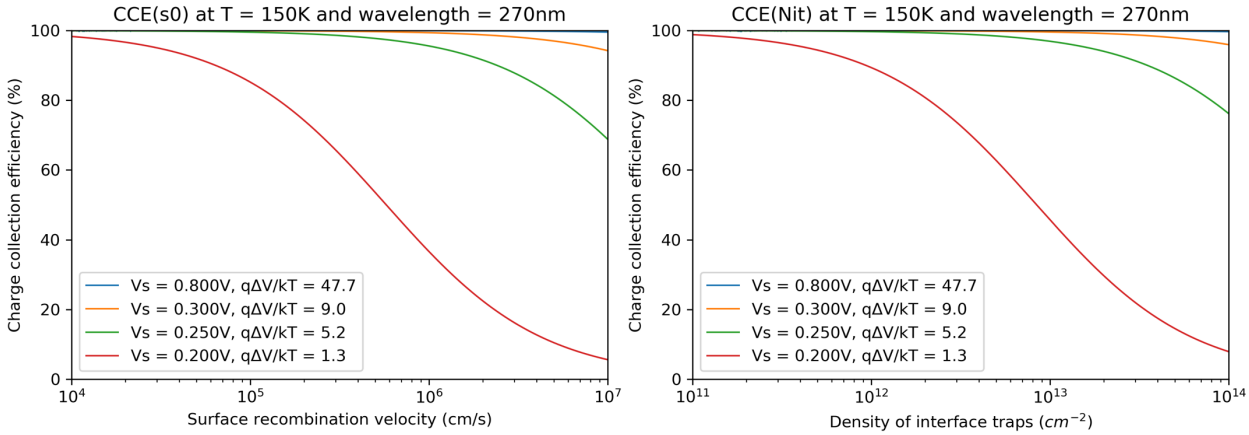

Figure 4: Strong surface passivation is required maintain QE-pinning in back-illuminated CCDs exposed to ionizing radiation. Radiation-induced surface damage is parameterized as the surface recombination velocity (plotted on the left) which is proportional to the density of interface traps (plotted on the right). The criteria for stable, QE-pinned sensitivity in a high radiation environment are $Vs \gg 0.3V$ and $q\Delta V/kT \gg 10$.

screened by radiation-induced traps, causing a flat band shift that degrades Vs with exposure to radiation. The relative stability of surface doping methods against radiation-induced traps is a major advantage in space-relevant environments, and a compelling reason to choose surface doping methods for space-borne instruments.

The surface recombination velocity is related to the trap density at the Si-SiO$_2$ interface [21]:

$$S_0 = N_{it} \cdot \sigma_{it} \cdot v_{th}(T) \qquad (15)$$

where N_{it} is the density of interface traps, σ_{it} is the capture cross section of the traps, and v_{th} is the thermal velocity of electrons in the detector. Values of S_0 less than 10^4 cm/s have negligible effect on quantum efficiency. Highly damaged surfaces can have $S_0 > 10^6$ cm/s. Following Albohn *et al.*, the cross section of the dangling bond (Pb0) trap at the Si-SiO$_2$ interface is on the order of 10^{-14} cm^2 [22]. With these parameters, and taking $v_{th} \sim 10^7$ cm/s, a surface recombination velocity $S_0 \sim 10^6$ cm/s corresponds roughly to an interface trap density of 10^{13} cm^{-2}.

With this relationship between surface recombination velocity and interface trap density, we can begin to define requirements for surface passivation in a space-relevant environment (Figure 4). In order to provide margin against radiation-induced surface traps, the surface passivation strength must be increased beyond the minimum necessary to stabilize the QE over the required temperature range. We therefore require that $Vs \gg 0.3V$ and $q\Delta V/kT \gg 10$ to meet requirements for end-of-life performance in space-relevant environments. Quantifying the margins required for stability would require an analysis of the radiation environment for a particular application. In the next section, we describe efforts to optimize ion implantation processes in a quest for stability in high radiation environments for spaceflight.

As one final comment on our models of QE(T) in weakly passivated CCDs, we note that the surface energy barrier depends on the bulk Fermi level, which as we have seen depends on the concentration of dopants in the detector epilayer, N_A. That being the case, the surface passivation strength can be improved without any change to the passivation process, simply by reducing the dopant density in the detector epilayer. The incremental increase in the energy barrier attained by this simple expedient can be significant (see Equation 10 for the relevant physics). Moreover, using higher purity silicon for the detector epilayer has the additional benefit of increasing the width of the front surface depletion layer, which improves detector resolution by limiting lateral diffusion of carriers in the field-free region of the detector. This observation applies to both backside charging and surface doping methods, and may be regarded as generally applicable to thinned detectors. There is a caveat to this approach. In weakly passivated detectors, depleting the detector to the back surface can reduce the effective energy barrier, potentially resulting in an unacceptable increase in dark current.

2.6 Ion-implanted CCDs and the quest for a stable EUV and soft X-ray detector

Early in their development of ion-implanted, back-illuminated CCDs, Stern *et al.* determined that in order to achieve high QE, the dopant gradient would have to be steep enough to achieve a surface electric field > 5x10^4 *V/cm*, while the surface

dopant density would have to be >5x10^{19}cm^{-3} in order to keep the width of the surface depletion region below 2 nm [23]. These requirements are difficult to achieve, and efforts to optimize ion-implantation processes for thinned CCDs would continue for more than a decade.

Optimization of ion implantation requires control over the dopant profile. The ability to control this profile precisely is limited by several process constraints, and a great deal of work has gone into optimizing ion-implanted detectors for space. The most important process parameters for forming shallow implant profiles are the implant dose and energy. Detectors must be annealed after implantation to activate the dopants and repair the damage to the silicon lattice. In semiconductor manufacturing processes, high temperature furnace anneals are available, but these processes are generally not compatible with frontside metals in CCDs. The solution to this problem is a laser annealing process, in which high intensity lasers are rastered across the CCD to melt the surface without causing significant heating at the front surface. These process requirements and constraints pose difficult challenges for the optimization of QE and stability in thinned CCDs.

Ion implantation and annealing processes described by Stern *et al.* (1994) were used in the manufacture of CCDs for the Extreme ultraviolet Imaging Telescope on the Solar and Heliophysics Observatory (SOHO-EIT) [24]. Launched on December 2, 1995, SOHO-EIT pioneered EUV observations of the sun and revolutionized our ability to forecast space weather. Unfortunately, the CCDs soon developed problems with QE degradation due to a combination of contamination and surface damage [25]. An in-depth study of the problem led to the conclusion that exposure to solar EUV radiation was causing local burn-in features that were traced to surface damage and charging [26-28]. The consequences of surface damage were reported as reduced QE and increased dark current, which were correlated with EUV exposure. Both QE and dark current recovered partially upon annealing. No evidence of QEH was reported.

The QE(T) model described in Section 2.4 provides metrics to explore the surface passivation strength in ion-implanted CCDs. Both the surface and bulk potentials vary with temperature in ion-implanted detectors, but the normalized energy barrier is independent of temperature. We see this from Equation 10, which shows that the energy barrier formed by ion implantation is proportional to the log of the ratio of surface and bulk dopant densities, $kT \cdot \ln(N_A^+/N_A)$. The stability requirement $q\Delta V \gg 10kT$ translates to a requirement on dopant densities, $N_A^+ \gg 10^5 N_A$. For a 20 Ω-cm detector, this means that the surface dopant density must be on the order of 10^{20}cm^{-3}, which is within the range explored by Stern *et al.* for soft X-ray and EUV CCDs [24]. Surface band structure calculations with nextnano++ show that dopant densities in this range are effective in suppressing QEH by effectively eliminating the backside potential well (Figure 5). Nevertheless, data and analyses of EUV-damage in SOHO-EIT CCDs suggest that the degradation of QE is caused by interactions of photogenerated charge with traps at the Si-SiO_2 interface. In their 1994 paper, Stern *et al.* developed a semi-empirical model for the charge collection efficiency (CCE) of ion-implanted CCDs, which parameterizes surface recombination in terms of the differential CCE as a function of depth from the back surface. The critical parameters in their model are the differential CCE at the back surface and the width of the ion-implanted layer. The differential CCE at the surface bears a striking resemblance to, and is certainly influenced by, the surface recombination velocity, which is proportional to the interface trap density (Equation 15). Provided that the surface dopant density is sufficiently high to prevent the formation of a backside potential well (see Figure 5), a radiation-induced increase in the local surface recombination velocity may therefore cause a local degradation of the QE without also introducing the instabilities associated with QEH.

The SOHO-EIT experience highlights the risk of surface damage caused by ionizing radiation in back-illuminated detectors. Sophisticated methods for radiometric calibration were developed to compensate for the effects of EUV-induced damage to the CCD surface, enabling useful scientific observations with EUV-damaged detectors [28]. The stability achieved with surface dopant densities in the range of 10^{20}cm^{-3} may have been essential to the success of this effort, but the difficulties in developing such a complicated model are prohibitive, and a better solution is needed. The CCE model in Stern *et al.* pointed to a way forward by calling for shallower implants to improve CCE. In their later work on CCDs for soft X-ray and EUV imaging, Stern *et al.* evaluated an EEV "enhanced" process that used shallower implants and steeper doping gradients to stabilize solar EUV imaging CCDs flown on GOES R and N [29, 30]. Stability was improved, but despite all the progress, 100% charge collection efficiency has not been achieved in ion-implanted CCDs.

2.7 Stability and QE in ion-implanted CCDs

The quest for stability in ion-implanted CCDs entails a tradeoff with UV sensitivity. The use of high surface dopant densities in the pursuit of greater stability results in a loss of sensitivity caused by recombination in the highly-doped, ion-implanted surface. Conversely, any attempt to optimize UV QE by reducing the surface dopant density compromises stability. Figure 5 illustrates the problem and the design trade. In the plots shown in Figure 5, electron wave functions are

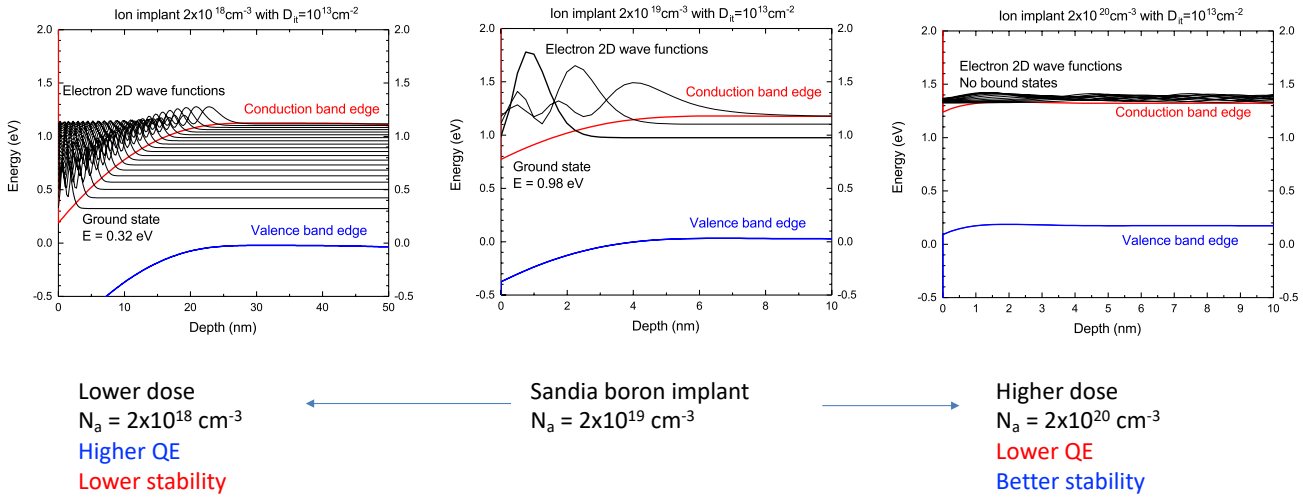

Figure 5: The tradeoff between UV quantum efficiency and stability of ion-implanted detectors is illustrated by nextnano++ calculations of surface electron states in the presence of Si-SiO_2 interface traps (see Figure 6 for comparison with 2D-doped detectors). While the stability of ion implanted detectors can be improved by increasing the surface dopant density, thereby eliminating bound states in the backside potential well (see plot on the right), the UV QE suffers from recombination in the highly doped silicon surface. Conversely, the UV QE may be improved by reducing the surface dopant density, but this leads to increased susceptibility to time-variable surface charge and QEH in radiation-damaged detectors.

superimposed on the near-surface conduction and valence bands in order to show the effect of surface doping on quantized electron energy states in the backside potential well. Electron states that are bound to the surface act as traps that can capture photoelectrons, leading to QEH. This problem can be avoided by doping the surface to a density in the range of 10^{20} cm^{-3}, thereby eliminating surface-bound electron states. Unfortunately, stability in high radiation environments comes at the expense of lower QE caused by Auger recombination in the highly doped surface.

This tradeoff between stability and QE in ion-implanted CCDs is illuminated by observations of QEH in the ion-implanted CCD43-80 detectors currently flying in Hubble's Wide Field Camera 3, which was launched in 2009 to replace WF/PC II on HST. Tests of the CCDs prior to launch revealed QEH at the level of a few percent [31-33]. While this low level of QEH represents a major advance over the instabilities that plagued WF/PC CCDs in the early days of HST, the residual instability still requires mitigation. To address this problem, HST periodically floods the WFC3 CCDs with visible light in order to fill surface traps and stabilize the response.

3. 2D-DOPED CCD AND CMOS DETECTORS FOR SPACEFLIGHT

3.1 Physics of 2D-doped CCDs: Stable, reflection-limited QE

In 1992, JPL reported the growth of delta-doped silicon by molecular beam epitaxy on CCDs for reflection-limited UV quantum efficiency [34]. A 2.5 nm layer of crystalline silicon was grown on fully-processed, back-thinned EG&G Reticon CCDs. Delta-doped CCDs contain an exceptionally high density of electrically-active boron ($2x10^{14}$ B/cm^2) in a single layer of the silicon crystal, which enables stable, uniform, reflection-limited QE. Delta-doped CCDs were shown to remain stable over a period of years independent of environmental conditions [35]. The Kepler group at NASA Ames measured the photometric precision of a delta-doped CCD, concluding that "the [delta-doped] CCD performed as a nearly shot-limited photometer with only a few ppm of error at an integrated flux of 10^{10} e^-" [36]. Near 100% internal QE in the soft X-ray and EUV spectral range was measured at the Stanford Synchrotron Radiation Laboratory (SSRL) [37].

The unique properties of 2D-doped silicon detectors are related to exceptionally high dopant densities, which are enabled by self-organization of dopant atoms during MBE growth. Delta-doping, first demonstrated at AT&T Bell Labs as a solution to the doping problem in silicon MBE, works by depositing dopant atoms on an atomically flat silicon surface, and then encapsulating the delta-doped layer by epitaxial growth of crystalline silicon. This process has been demonstrated

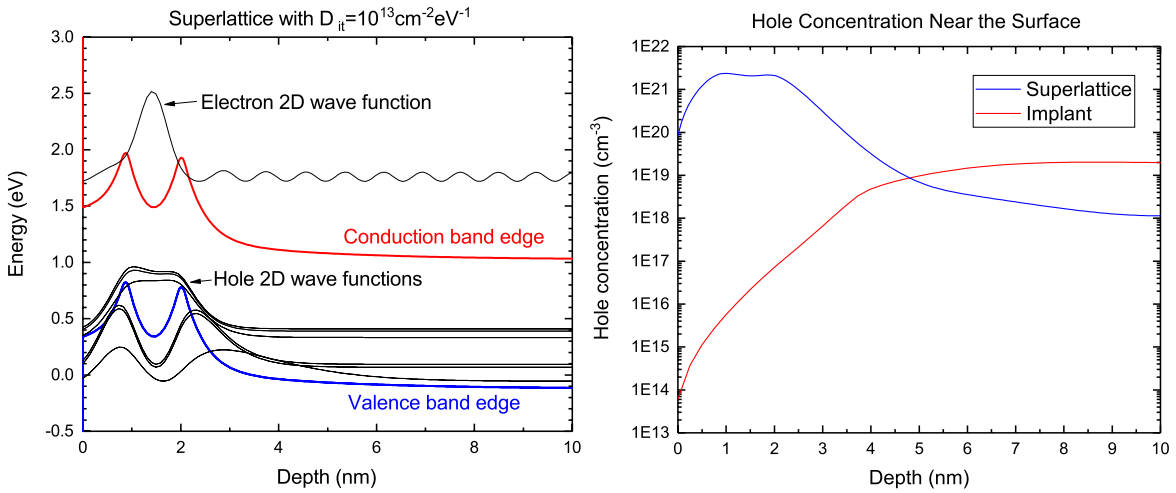

(6a) Quantum confinement in a 2D-doping superlattice

(6b) Near-surface hole concentration

Figure 6: Quantization of near-surface electron and hole states plays an essential role in the physics and stability of 2D-doped silicon detectors [43-45]. Electron and hole wavefunctions represented here were calculated using nextnano++, which solves the Schrödinger and Poisson equations self-consistently for nanostructured semiconductor devices [46]. This figure shows that the surface of a 2D-doped detector is strongly accumulated, with a surface effective bandgap > *1.5 eV*.

at surface densities up to half a monolayer of dopant atoms (*i.e.*, up to $3.4 \times 10^{14} cm^{-2}$ on Si (100)) [38-42]. Dopant concentrations more than an order of magnitude higher than the solid solubility limit of conventional 3D-doping methods are possible because self-organization and geometric frustration prevent dopant atoms from occupying nearest-neighbor sites in the 2D-doped surface [41, 42]. Electrically active dopant concentrations up to $10^{22} cm^{-3}$ with mobilities of 20 cm^2/Vs have been reported in boron delta-doped silicon, and full dopant activation and metallic conduction have been reported in delta-doped silicon at temperatures as low as 4K [40]. Quantization of near-surface electron and hole states in 2D-doped surfaces is illustrated in Figure 6 [43-45]. One result of this quantization is an increase in the effective band gap of the 2D-doped surface, as the near-surface Fermi level is driven deep into the valence band (Figure 6). Quantization of surface hole states also leads to a high density of holes in 2D-doped surfaces, which suppresses surface dark current and persistence for exactly the same reasons cited by Janesick for front- and back- surface passivation of CCD interfaces [13].

3.2 2D-doping processes

The invention and early development of delta-doped CCDs was accomplished with a 3" Riber MBE system that could only process one detector at a time. Detectors were prepared using a frame-thinning process, which only removes the substrate in the imaging area, while leaving the edges of the detector thick enough to support the membrane. Unfortunately, frame-thinned CCDs are prone to significant warping of the imaging surface due to residual stresses in the front side oxides and gate structures. The utility of these early devices for scientific imaging was therefore severely limited by poor surface flatness, and by the inability to scale the frame-thinning process to the large, buttable devices needed by astronomers. To solve this problem, JPL's Microdevices Laboratory installed and commissioned a first-of-its-kind Veeco GEN200 silicon MBE system in our clean room facilities, together with supporting equipment for wafer-scale surface preparation. The computer-controlled MBE system is equipped with a robotic system for automated transfer of wafers under ultra-high vacuum (UHV) between a cluster chamber and a separate growth chamber. JPL's investment in a production-scale molecular beam epitaxy (MBE) system has given us the ability to process 150mm and 200mm silicon detector wafers with high throughput and high yield (Figure 7).

The 2D-doping process begins with planarization and oxide-oxide bonding of detector wafers. After bonding, the device wafers are thinned to expose the detector epilayer for back illumination. The thinning process begins with a grinding process for coarse thinning, followed by a chemical etch (1:3:8 $HF:HNO_3:H_2O$) to selectively remove the highly-doped silicon substrate. After substrate removal, a chemical-mechanical polish removes additional silicon, leaving the wafer with a uniform, mirror finish with nanometer-scale surface roughness. Wafers are prepared using standard cleaning processes to remove organic and metallic contaminants. The final surface preparation steps prior to MBE growth nitrogen-purged

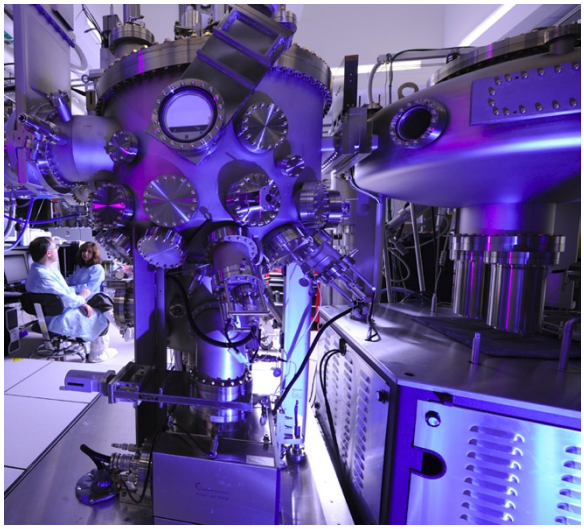

(7a) Production-scale silicon MBE system

(7b) 200mm wafer with CMOS detectors in the MBE chamber

Figure 7: JPL's investment in a Veeco GEN200 silicon MBE system enables high volume manufacturing of 2D-doped detectors. The photograph on the right shows a bonded and thinned 200mm detector wafer in the MBE chamber. Although the surface in the photograph comprises bare, atomically clean silicon ready for MBE growth, at an overall thickness of about 3 microns, the silicon epilayer is thin enough that front-surface detector structures are visible through the partially-transparent silicon epilayer.

glove box. A UV-ozone process removes residual carbon contamination, and the native oxide is removed with a spin-clean process originally developed by Paula and Frank Grunthaner at JPL for low temperature MBE [47].

Eight wafers at a time can be loaded into the MBE system. Detector wafers are placed face-down on 10 inch platens and loaded into an elevator in the introduction chamber of the Veeco MBE system. The introduction chamber is then evacuated using a clean cryopump system, and wafers are robotically transferred into a UHV cluster chamber, where they are loaded into an 8-position elevator for temporary storage. Wafers are transferred one at a time into a separate UHV chamber for MBE growth. The MBE growth chamber is equipped with a radiative substrate heater for controlling the wafer temperature, an e-beam source for deposition of silicon, and multiple effusion cells for deposition of dopants. All sources are equipped with shutters. Epitaxial growth of 2D-doped silicon is performed by controllably heating the wafer to between 400°C and 425°C. When the substrate temperature rises above 370°C, the atomic structure of the silicon surface changes from di-hydride to monohydride termination of silicon, which is a necessary condition for epitaxial growth. Growth of 2D-doped silicon proceeds by alternately depositing silicon and dopant atoms, using shutters to control the source fluxes. Under these conditions, silicon and dopant atoms are integrated into the silicon lattice, forming an epitaxial layer of silicon with atomic layer control over the dopant profile. The atomically abrupt "delta-doped" structure is formed by closing the silicon shutter and opening the dopant shutter in order to deposit a fraction of a monolayer of dopant atoms on the atomically-flat silicon surface [34, 35, 38-42]. Once this layer is formed, the dopant shutter is closed and the silicon shutter is opened to resume epitaxial growth of silicon.

3.3 Optimization of MBE growth processes and surface passivation strength in 2D-doped detectors

Soon after JPL transitioned to 2D-doping at full wafer scale, we upgraded our delta-doping process to multilayer 2D-doping in order to improve the strength and stability of detector passivation for high radiation environments [43-45]. The 2D-doping superlattice comprises a series of stacked delta-doped layers. Although the total thickness of the 2D-doping superlattice is only a few nanometers, this multilayer structure can contain an integrated dopant density that's comparable to or greater than the integrated dopant density in the ion-implanted surfaces used to passivate state-of-the-art back-illuminated CCDs and CMOS imaging detectors, while still achieving stable, near 100% charge collection efficiency.

Early results from this work were very promising. Lifetime tests performed on 2D-doped CMOS detectors showed unique stability against radiation-induced surface damage, and QE measurements showed nearly 100% charge collection efficiency with wafer-scale 2D-doping processes. Figure 8 shows a 2D-doped CMOS wafer with CMV12K devices after bonding, thinning, and MBE/ALD passivation [48]. These 3kx4k super high definition CMOS detectors were designed by

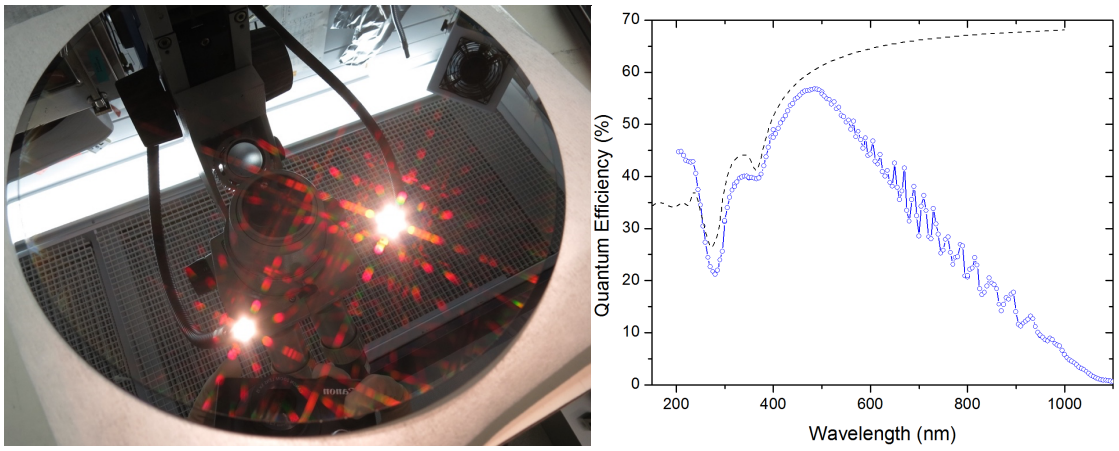

Figure 8: Measured quantum efficiency of back-illuminated, superlattice-doped CMV12000 device [48]. With a charge collection efficiency of approximately 90%, this detector is nearly QE-pinned, but the difference may indicate weak surface passivation due to damage to the detector from the thinning process. See text for discussion.

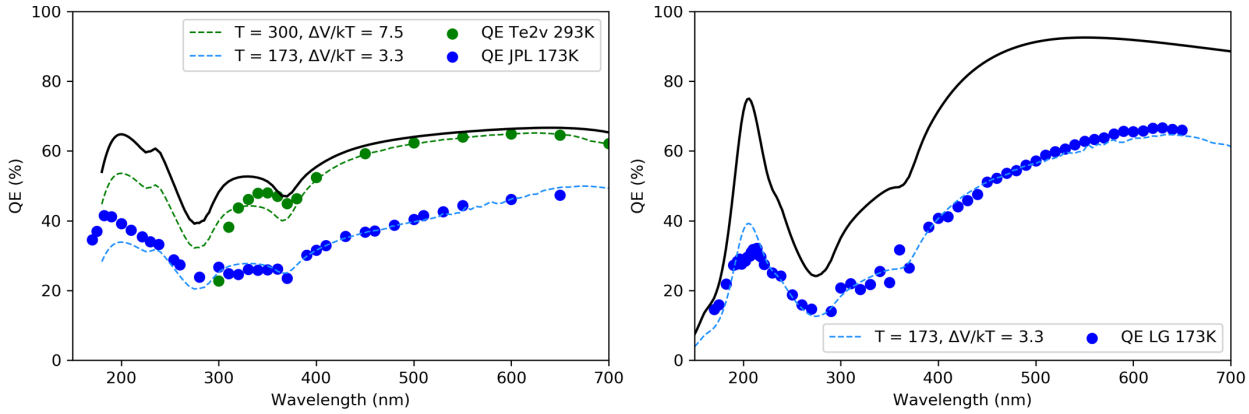

Figure 9: This figure shows that MBE growth on CMP-damaged detectors leads to weak surface passivation. Although nearly QE-pinned at room temperature, at -100°C the QE of these two CCDs is ~2x below the reflection limit across the entire spectral range from UV to visible. This degradation of QE with temperature closely matches QE(T) calculations based on the model developed in Section 2, with $V_S \approx 0.2V$ and $S_0 \approx 3 \times 10^6\ cm/s$.

CMOSIS and fabricated by TowerJazz on 200mm wafers using a 0.18 µm process. Novati bonded the wafers to a 200mm silicon wafer for mechanical support. JPL performed final thinning and surface passivation at full wafer scale using an MBE-grown 2-layer superlattice. Finally, JPL used atomic layer deposition to grow a 2nm Al_2O_3 layer on the back-illuminated surface. Metrological measurements indicate the final device thickness was between 2 and 3 µm. For reference, the optical transmittance of silicon with a 2nm Al_2O_3 coating is plotted as a dashed line. The observed falloff in quantum efficiency and interference fringes at wavelengths longer than 500 nm are consistent with the measured 2 to 3 µm thickness of devices after thinning. At short wavelengths (below ~300nm), the QE exceeds the optical transmission into silicon, which is consistent with multiple electron-hole pair production by high energy photons. The difference between the silicon transmittance and the measured QE suggests that about 90% of UV photons are detected.

While the QE of this detector is very high, the difference between 90% and 100% CCE may indicate a latent problem. The QE data shown in Figure 8 were measured at room temperature. Low temperature QE measurements in Figure 9 unexpectedly revealed a strongly temperature-dependent QE in some detectors that were processed at full wafer scale. As we showed in Section 2, QE(T) is a signature of weak passivation, and in fact the dashed lines in Figure 9 were calculated using the model developed in Section 2. The QE(T) model matches the data for a combination of low surface potential (V_S~0.2V) and high surface recombination velocity (S_0~3x10^6cm/s), which suggests that the integrated trap density in these detectors is very high. The model indicates that the energy barrier varies from 8.1kT at room temperature to 3.8kT at 173K, in apparent contradiction with the calculated band structure of 2D-doped detectors (see Figure 6). Resolving this apparent contradiction requires a change in perspective. The data and the model point to a high density of traps, but the

traps are not located at the Si-SiO_2 interface. Weak passivation in these detectors is caused by defects in the detector surface, not the Si-SiO_2 interface. We were finally able to trace the traps to the chemical-mechanical polishing (CMP) process used during thinning. Although defects in CMP-prepared surfaces are difficult to detect, near-surface silicon vacancies have been observed [49-51]. One interesting aspect of this change in perspective is an explanation for the fact that the QE of CMP-damaged detectors is stable and amenable to calibration, provided the detector temperature remains stable. The problem was solved by etching the detector surface to remove CMP-damaged silicon before MBE growth.

The surface band structure of CMP-damaged detectors provides insight and inspiration for further optimization of the 2D-doping process. A comparison of QE data, nextnano++ models of CMP-damaged detectors, and our QE(T) model shows that the defects are very shallow, within a few nanometers of the MBE-detector interface (Figure 10). Such a thin damaged layer would ordinarily have been removed in the standard silicon cleaning process, which both cleans and etches the silicon surface. Unfortunately, some of our oxide-oxide bonded wafers suffered catastrophic delamination during cleaning, and we were forced to curtail the exact cleaning step that would have eliminated the CMP damage. Once we identified the cause of the QE(T) problem, we modified our cleaning process to include an old, but very effective, surface etch after the final CMP step [52]. Takizawa's "slight etch" method successfully removed the damage and solved the problem.

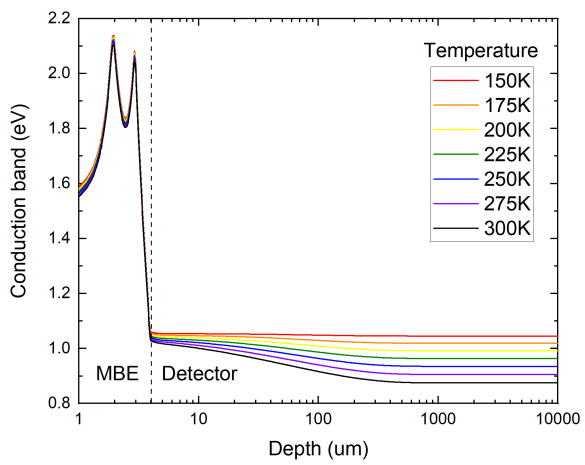

(10a) Conduction band edge, N_{it} = 5x10^{13}cm^{-2}

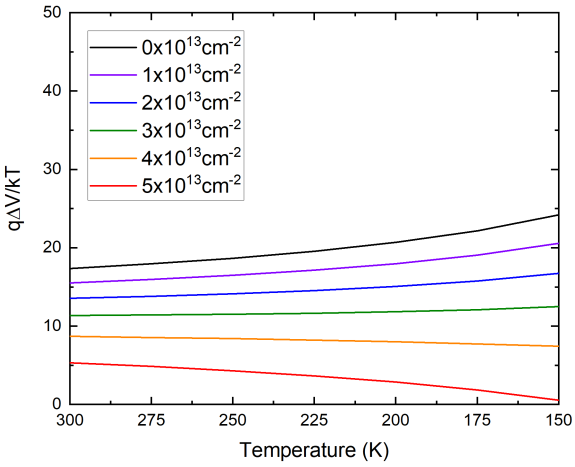

(10b) Barrier vs T for various damage densities

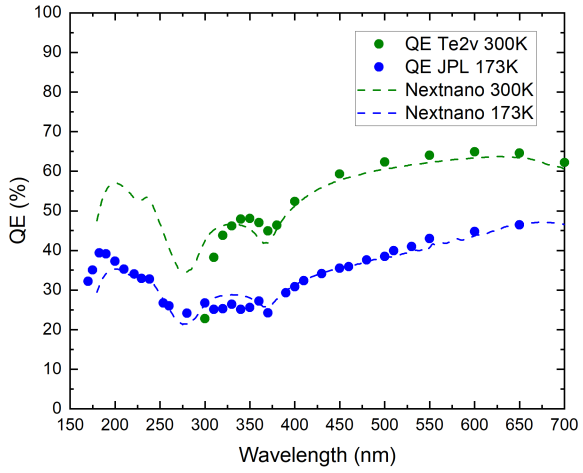

(10c) Calculated QE of CMP-damaged CCD #1

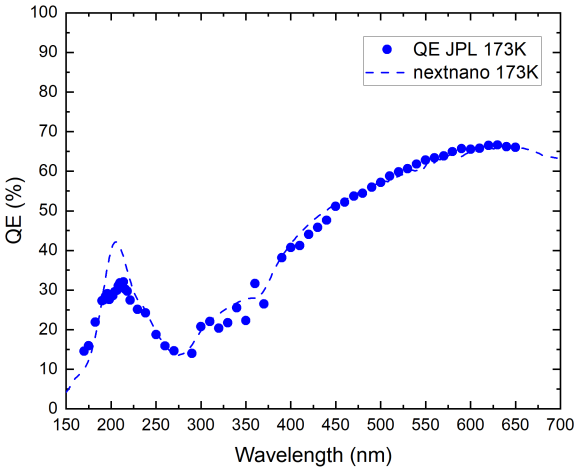

(10d) Calculated QE of CMP-damaged CCD #2

Figure 10: Correlations of detector data, nextnano++ band structure calculations, and QE(T) models suggest that CMP damage comprises a very shallow distribution of traps with integrated density on the order of 5x10^{13}cm^{-2}. Nextnano++ band structure calculations (Figures 10a and 10b) were used as inputs to the QE(T) model described in Section 2, and the trap density was adjusted to reproduce the temperature-dependent QE observed in damaged detectors (Figure 10c and 10d).

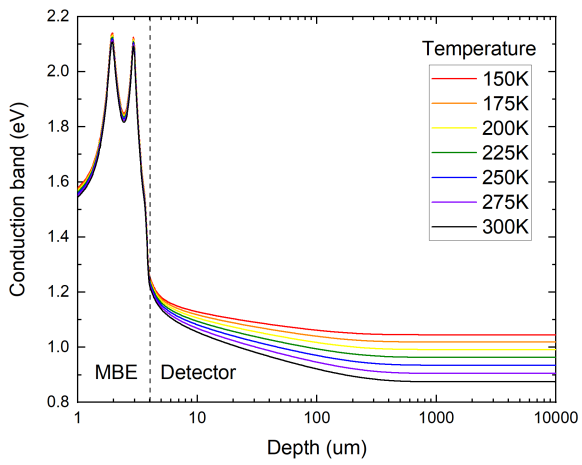

(11a) 3-layer superlattice, Nit = $5x10^{13}cm^{-2}$

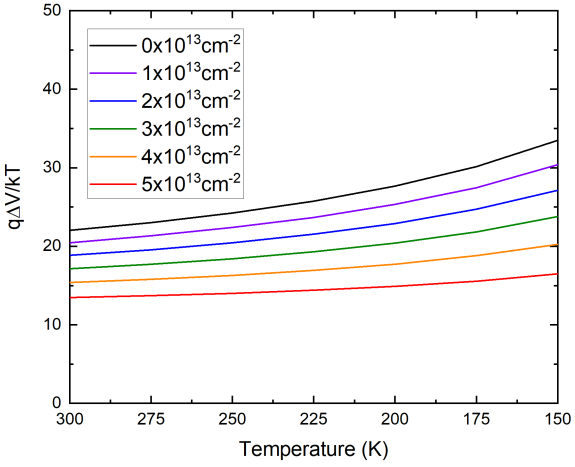

(11b) Barrier height (T) in 3-layer superlattice

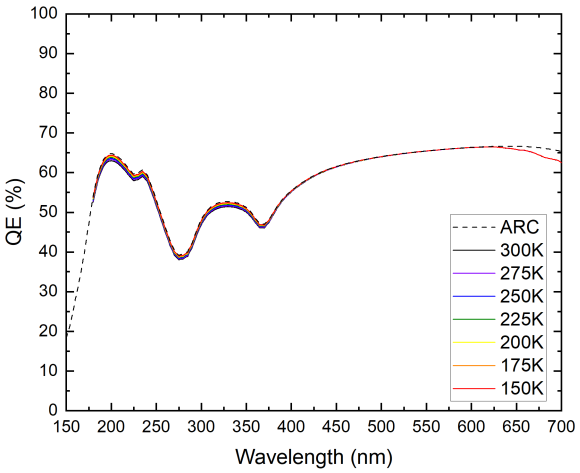

(11c) Calculated QE of CMP-damaged CCD #1

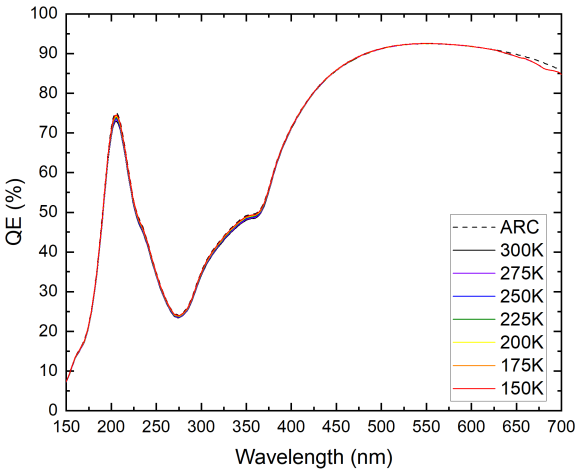

(11d) Calculated QE of CMP-damaged CCD #2

Figure 11: Optimization of the MBE layer structure by adding a third delta layer located as close as possible to the MBE-detector interface significantly improves the strength of surface passivation relative to the 2-layer superlattice modeled in Figure 10. Even for exceptionally high trap densities ($5x10^{13}cm^{-2}$ was assumed here), the detector remains QE-pinned over the full temperature range relevant to space.

Our resolution of this problem had two positive outcomes. Changing our focus from the Si-SiO_2 interface to the MBE-detector interface motivated us to not only improve our surface cleaning processes, but also to optimize the structure of the 2D-doping superlattice. Ever since our first MBE growth of delta-doped silicon on a thinned CCD surface in 1991, we had always begun by growing a silicon buffer layer approximately 1nm in thickness. The use of buffer layers in MBE growth is standard practice, serving to encapsulate any contaminants or defects that may remain on the surface, and to form an atomically clean and smooth surface conducive to high quality crystalline growth. Our discovery of QE(T) resulting from growth on CMP-damaged detectors revealed a latent problem with this process, insofar as the thickness of the buffer layer amplifies the effect of defects and contaminants on detector QE. With this in mind, we tested the possibility of using a third delta layer, positioned as close to the MBE-detector interface as possible, in order to compensate any charge trapped near the detector surface. These tests were successful, and we've now incorporated a third delta layer in an enhanced 2D-doping process. Using nextnano++ models of surface band structure as inputs to the QE(T) model, we were able to reproduce the QE(T) data in CMP-damaged detectors (Figure 10). Similar calculations for a 3-layer superlattice illustrate the enhanced QE achieved by optimizing the 2D-doping process (Figure 11). Whereas these calculations show that our enhanced 2D-doping process is highly insensitive to traps at the MBE-detector interface, we have to shift our focus back to the Si-SiO_2 interface to study radiation hardness of 2D-doped detectors in a space-relevant environment.

3.4 Experimental evidence for the stability and radiation hardness of 2D-doped detectors

Experimental proof of the stability and radiation-hardness of 2D-doped detectors is described in references [44] and [45], in which data are presented from DUV lifetime measurements of 2D-doped CMOS image sensors. Over the course of several months, our collaborators at Alacron and Applied Materials exposed 2D-doped CMOS detectors to high intensity, pulsed lasers at 193nm and 263nm. Despite suffering high levels of DUV-induced damage to the Si-SiO_2 interface, the QE of 2D-doped CMOS detectors remained stable to a precision of 1%, with no measurable persistence or degradation of resolution. As described in Section 3.1, quantum confinement of holes in the 2D-doped superlattice contributes to the stability of 2D-doped detectors against radiation-induced degradation of the Si-SiO_2 interface by suppressing generation and recombination at the Si-SiO_2 interface.

The stability of 2D-doped detectors in high radiation environments has inspired collaborations between JPL and high energy physicists on the development of a soft X-ray imager using 2D-doped CMOS detectors [53-55]. The PERCIVAL collaboration needed detectors with high stability and QE to detect soft X-rays for high-energy physics experiments, and performed extensive characterization of our detectors using synchrotron radiation at DESY. Detailed characterization of 2D-doped CMOS detectors was performed for single-photon event detection with high sensitivity and resolution. Charge collection efficiencies of 90% were measured in the 100-300eV energy range.

In a collaboration between JPL and Sandia National Laboratories (SNL), 2D-doped silicon photodiodes were fabricated and characterized for high-speed detection of soft X-rays in the high radiation environments of the SNL Z-machine [56,57]. The detector structure comprised fully-depleted photodiodes with highly-doped surfaces. In order to handle the high-intensity X-ray pulses created by the Z-machine, a high surface conductivity is required. Three types of photodiodes were fabricated and compared. Photodiodes passivated with SNL's standard ion-implantation process served as the control. Two types of 2D-doped photodiodes were fabricated, one that combined 2D-doping with SNL's ion implantation process, and another with a 2D-doped surface alone. The results of this experiment illuminate the qualitative as well as quantitative differences between 2D-doping and ion implantation. The QE of ion-implanted detectors suffers from losses due to both surface and bulk recombination (Figure 12). In the superlattice+implant detector, surface recombination is eliminated, resulting in a ~2x improvement in UV QE relative to the ion-implanted device. In the superlattice-only detector, both surface and bulk recombination are eliminated, resulting in a ~4x improvement in UV QE. From these data we can infer that surface and bulk recombination are roughly equally important in Sandia photodiodes. Sandia's detectors were designed for use in the high-radiation environment of the Sandia Z-machine. Scientific detectors designed for low flux UV measurements in space have different environmental requirements, potentially leading to an emphasis on QE over stability.

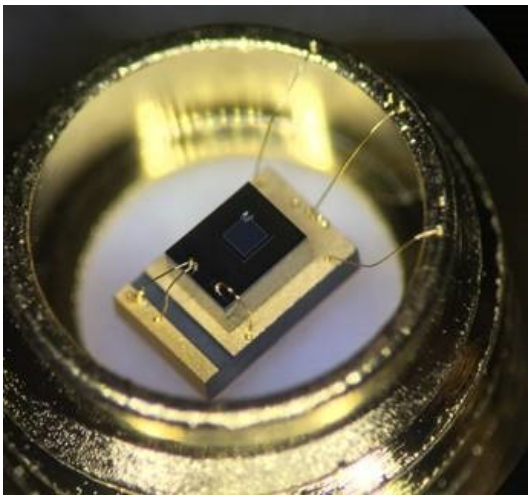

(12a) Sandia fully depleted photodiode

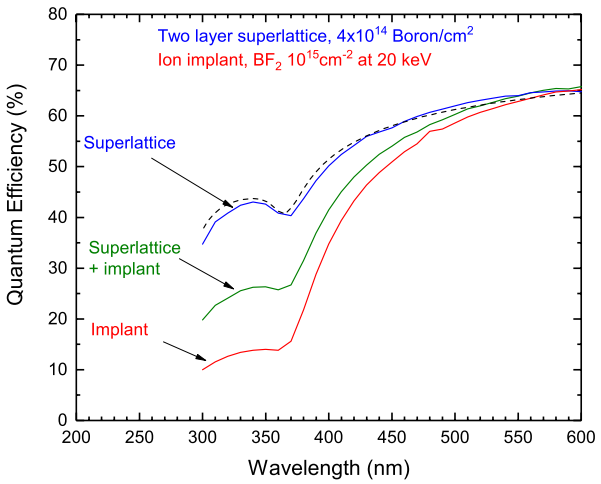

(12b) UV QE of ion implanted and 2D-doped detectors

Figure 12: Comparison of the fully-depleted Sandia photodiodes with three different surface dopant profiles shows 2D-doping enables significantly higher UV quantum efficiency [34,35]. Data show that 2D-doped superlattices enable the highest quantum efficiency, nearly equal to the reflection limit (shown as a dashed line in the figure). The UV quantum efficiency of the superlattice+implant detector is about 2x lower, and the UV quantum efficiency of the implant-only device is about 4x lower. These data provide quantitative estimates of surface and bulk losses in ion-implanted detectors (see text).

3.5 Flight heritage and technology readiness of 2D-doped imaging detectors

JPL has made significant advances in the technology readiness of 2D-doped detectors with detector-integrated coatings and filters for spaceflight [58-68]. Detector-integrated UV bandpass filters represent a science- and mission- enabling technology for silicon detectors, providing essential capabilities for the detection of faint FUV and NUV signals in the presence of visible and near-IR sky backgrounds. Processes and data for precise deposition of single- and multilayer antireflection coatings and metal-dielectric UV bandpass filters on 2D-doped detectors are described elsewhere [59-65]. We have flown 2D-doped CCDs with integrated antireflection coatings in suborbital balloon and rocket experiments, and will soon deliver a camera with 2D-doped CCD47 detectors in the FUV and NUV channels of the Star-Planet Activity Research CubeSat (SPARCS) [66-68].

JPL and Teledyne-e2v recently formed a strategic partnership with the goal of offering 2D-doping as a space-qualified processing option for Teledyne's range of scientific detectors. In order to achieve this goal, we have selected electron multiplying CCD201 detectors and large format CCD272 detectors as vehicles for process qualification, on the basis that these detectors have been qualified for spaceflight and are representative of the range of Teledyne e2v's CCD fabrication processes. Wafer lots comprising CCD201 and CCD272 detectors are being delivered to JPL for bonding, thinning and 2D-doping. Fully-processed, 2D-doped detector wafers are delivered to Teledyne e2v for probing, dicing, packaging, and characterization. Process qualification will include Teledyne e2v's standard suite of lot qualification tests in space-relevant environments. Work on this project began in 2019 and is currently underway.

Two CCD201 detectors processed using our enhanced 2D-doping process were delivered to Open University for testing. Most of the detectors on this wafer were damaged during thinning, resulting in critical metal traces being severed, but fortunately these detectors retained sufficient functionality for QE testing. The processing problem has been resolved, and additional wafers are currently being processed. When processing of the next batch of CCD201 wafers is complete, we plan to perform Teledyne e2v's full suite of lot acceptance testing for flight detectors, including tests of durability in space-relevant environments.

The QE data from these first 2D-doped CCD201 detectors are very promising. QE measurements were performed at Open University using a UV-enhanced Te2v CCD97 as a calibrated standard [69]. Measurements were performed using a Thorlabs Deuterium source, with UVFS and CaF_2 lenses and glasses for UV transmission. Spectral data were measured using filters spanning the range 193-420 nm, with 10 nm bandwidth. Both of the 2D-doped detectors exhibited near 100% charge collection efficiency, with 3x higher QE than the UV-enhanced CCD97 at 270nm, and more than 2x higher QE throughout the near UV spectral range (Figure 13). The QE of 2D-doped CCD201 detectors is stable and uniform over the temperature range +20°C to -40°C (Figure 14).

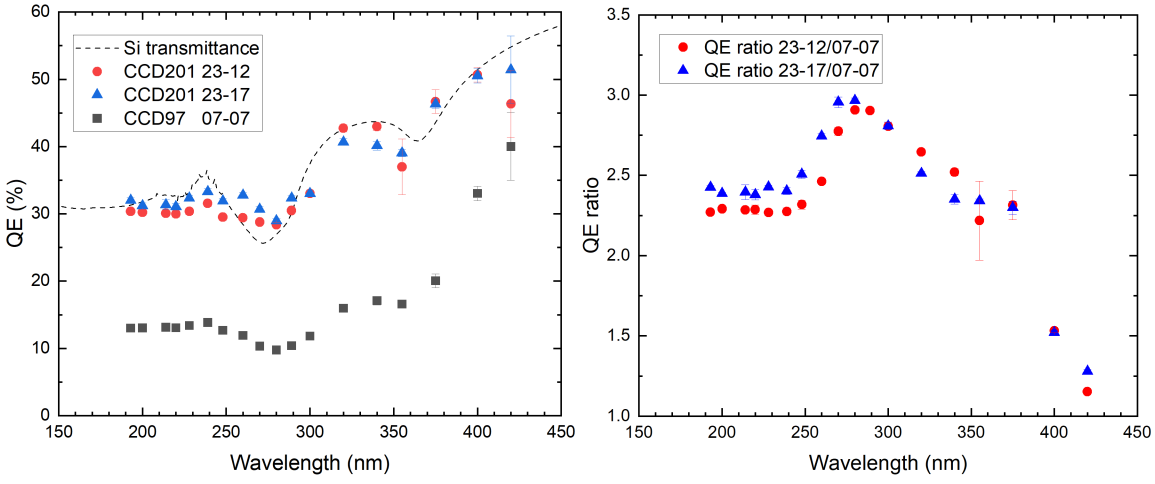

(13a) Stability over temperature

(13b) Uniformity over the detector

Figure 13: Measured quantum efficiency of 2D-doped CCD201 detectors in comparison with a Te2v UV-enhanced CCD97. QE data for the CCD201 detectors were measured relative to a calibrated CCD97 detector that was extensively characterized by Heymes *et al.* 2020 [69] (Figure 13a). The 2D-doped detectors exhibited nearly 100% charge collection efficiency over the range measured, with 2x to 3x improvement in UV QE compared to the UV-enhanced CCD97 (Figure 13b).

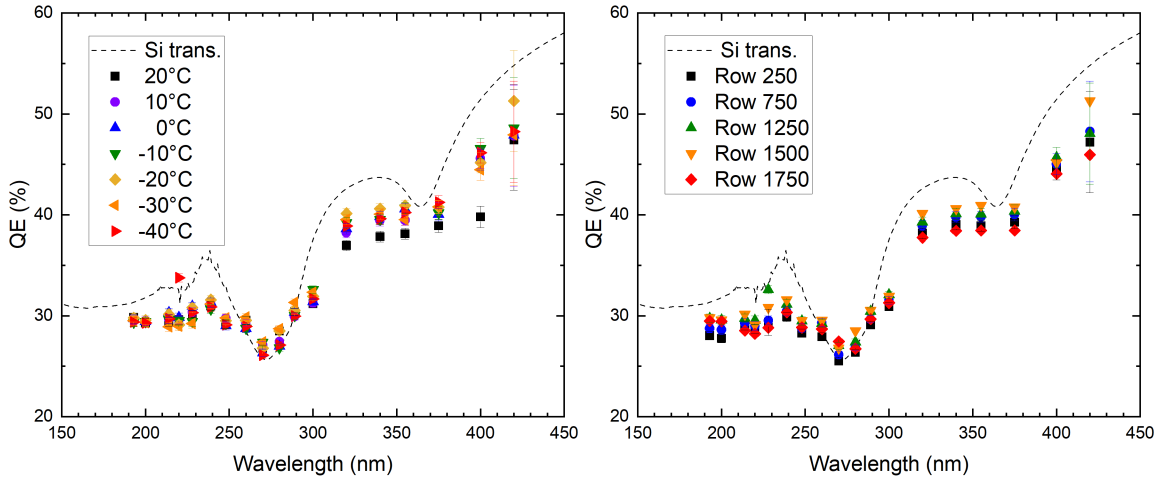

(14a) Stability over temperature

(14b) Uniformity over the detector

Figure 14: These data show that the QE of 2D-doped CCD201 detectors remains stable over temperature (Figure 14a) with uniform response across the detector (Figure 14b). The slight decrease in QE at room temperature may be due to higher dark current at this temperature.

4. SUMMARY

We reviewed the history and physics of back-illuminated CCDs. The discovery of quantum efficiency hysteresis in CCDs on the Hubble Space Telescope motivated efforts to develop stable surface passivation methods for thinned CCDs. Weakly passivated CCDs suffer low, temperature-dependent quantum efficiency. Starting with Morley Blouke's model of thinned CCDs, we developed an algorithm for calculating QE(T) in weakly passivated detectors, and then applied this model to derive requirements for strong surface passivation in space-relevant radiation and thermal environments. The strength of surface passivation is parameterized in terms of energy, as opposed to earlier surface passivation models based on the strength of the near-surface electric field. The QE(T) model proved useful in comparing the effects of temperature, epilayer doping, and Si-SiO_2 interface traps on the stability of various surface passivation technologies. Using nextnano++ software to model the near-surface band structure of thinned detectors, we showed how quantization of electron and hole states plays an essential role in the stability and strength of surface passivation in 2D-doped detectors. Data and models of thinned detectors were used to compare surface passivation processes, leading to the conclusion that 2D-doping provides the highest surface passivation strength and radiation hardness of any available process for passivating thinned CCDs and CMOS detectors in space-relevant radiation and thermal environments. Comparisons with ion-implanted CCDs in this and previous programs show that 2D-doping enables 2x to 3x higher UV QE than ion-implanted CCDs. Lifetime tests with pulsed DUV and excimer lasers show that 2D-doped detectors are uniquely hardened against surface damage caused by ionizing radiation. A strategic partnership between JPL and Teledyne e2v for the certification of JPL's processes for manufacturing flight-qualified, 2D-doped CCDs is discussed, including preliminary data showing that our enhanced 2D-doping process enables stable, uniform, reflection-limited UV QE.

ACKNOWLEDGMENTS

The research was carried out in part at the Jet Propulsion Laboratory, California Institute of Technology, under a contract with the National Aeronautics and Space Administration.

REFERENCES

[1] *Pathways to Discovery in Astronomy and Astrophysics for the 2020s*, National Academies Press, Washington DC (2021)

[2] Shortes, S. R., Chan, W. W., Rhines, W. C., Barton, J. B., and Collins, D. R., "Characteristics of thinned backside-illuminated charge-coupled device imagers," *Applied Physics Letters*, 24(11): 565-567 (1974).

[3] Blouke, M. M., Cowens, M. W., Hall, J. E., Westphal, J. A., and Christensen, A. B., "Ultraviolet downconverting phosphor for use with silicon CCD imagers," *Applied Optics*, 19(19): 3318-3321 (1980).

[4] Trauger, J. T., "Sensors for the Hubble Space Telescope wide field and planetary cameras (1 and 2)," *CCDs in astronomy; Proceedings of the Conference,* Tucson, AZ, Sept. 6-8, 1989 (A91-45976 19-33). San Francisco, CA, Astronomical Society of the Pacific, p. 217-230, (1990).

[5] Blouke, M. M., Janesick, J. R., Hall, J. E., and Cowens, M. W., "Texas Instruments (TI) 800X800 Charge-Coupled Device (CCD) Image Sensor," *Proc. SPIE 0290*, *Solid-State Imagers for Astronomy*, (1 January 1981); doi: 10.1117/12.965830

[6] Griffiths, R. E., Ewald, S. P., and MacKenty, J. W., "The Operational Optimisation of the TI 3-phase CCD in the Hubble Space Telescope," *CCDs in astronomy; Proceedings of the Conference*, Tucson, AZ, Sept. 6-8, 1989 (A91-45976 19-33). San Francisco, CA, Astronomical Society of the Pacific, p. 231-236, (1990).

[7] Robinson, L. B., "A review of surface treatment for CCD's," ESO/OHP Workshop on the Optimization of the Use of CCD Detectors in Astronomy (1986).

[8] Janesick, J., Elliott, T., Daud, T., McCarthy, J., and Blouke, M., *"*Backside charging of the CCD*," SPIE Proc.*, Vol 570 Solid State Imaging Arrays (1985).

[9] Janesick, J., Elliott, T., Fraschetti, G., Collins, S., Blouke, M. and Corrie, B. "Charge-Coupled Device Pinning Technologies," Proc. SPIE 1071, Optical Sensors and Electronic Photography, (1989); doi:10.1117/12.952516

[10] Janesick, J., Elliott, T., Daud, T., and Campbell, D., "Flash Technology for CCDs," *Opt. Eng.* 26(9): 852-863 (1987).

[11] Lesser, M., and Iyer, V., "Enhancing back illuminated performance of astronomical CCDs," *SPIE Proc.*, Vol. 3355, pp. 436-456 (1998).

[12] Blouke, M. M., "Model of a thinned CCD," Proc. SPIE 1439, International Conference on Scientific Optical Imaging, (1 December 1991); doi:10.1117/12.50465

[13] Janesick, J. R., *Scientific Charge-Coupled Devices / James R. Janesick, Editor.* SPIE Press (2001). doi:10.1117/3.374903

[14] Misiakos, K., and Tsamakis, D., "Accurate measurements of the silicon intrinsic carrier density from 78 to 340 K," *Journal of Applied Physics* 74: 3293 (1993); https://doi.org/10.1063/1.354551

[15] Varshni, Y. Pl, "Temperature dependence of the energy gap in semiconductors," *Physica*, 34(1): 149-154 (1967).

[16] Mane, R., Ly, I., Wade, M, Datta, I., Douf, M. S., Traore, Y., Ndiaye, M., Tamba, S., and Sissoko, G., "Minority Carrier Diffusion Coefficient D*(B,T): Study in Temperature on a Silicon Solar Cell under Magnetic Field," *Energy and Power Engineering,* 9(1): 1-10 (2017).

[17] Schmidt, J., Veith, B., Werner, F., Zielke, D., and Brendel, R., "Silicon surface passivation by ultrathin Al2O3 films and Al_2O_3/SiNx stacks," *2010 35th IEEE Photovoltaic Specialists Conference*, pp. 000885-000890, doi: 10.1109/PVSC.2010.5614132. (2010)

[18] Li, F, Nixon, O, and Nathan, A, "CCD Detection of 157 nm photons," *Proc. IEEE Workshop on Charge-Coupled Devices and Advanced Image Sensors*, Elmau, Germany (2003).

[19] Li, FM, and Nathan, A, *CCD image sensors in deep-ultraviolet: degradation behavior and damage mechanisms*, Springer, Berlin (2005).

[20] Arp, U., Shaw, P.S., Gupta, R. and Lykke, K.R., "Damage to solid-state photodiodes by vacuum ultraviolet radiation," *J. Electron Spectroscopy and Related Phenomena*, **144-147**: 1039-1042 (2005).

[21] Sze, S. M., *Physics of Semiconductor Devices, Second Edition*, John Wiley and Sons, New York (1981).

[22] Albohn, J., Füssel, W., Sinh, N. D., Kliefoth, K., and Fuhs, W., "Capture cross sections of defect states at the Si-SiO_2 interface," *Journal of Applied Physics* 88, 842 (2000); https://doi.org/10.1063/1.373746

[23] Stern, R. A., Catura, R. C., Kimble, R., Davidsen, A. F., Winzenread, M., Blouke, M. M., Hayes, R., Walton, D. M., and Culhane, J. L., "Ultraviolet and extreme ultraviolet response of charge-coupled device detectors," *Optical Engineer*ing, 26(9): 875-883 (1987).

[24] Stern, R. A., Shing, L., and Blouke, M. M., "Quantum efficiency measurements and modeling of ion-implanted, laser annealed charge-coupled devices: x-ray, extreme-ultraviolet, ultraviolet and optical data," *Appl. Optics* 33, pp. 2521–2533 (1994).

[25] Defise, J.-M., Clette, F., Moses, J. D., Hochedez, J.-F. E., "In-orbit diagnostic of the EIT EUV CCD radiation induced aging," *SPIE proc.* 3114 (1997).
[26] Defise, J.-M., Moses, J. D., Clette, F., and the EIT Consortium, "In-orbit performances of the EIT instrument on-board SOHO and intercalibration with the EIT Calroc Sounding rocket program," *Proc. SPIE*, 3442, 126–139 (1998).
[27] Defise, J.-M., Clette, F., and Auch`ere, F., "In-flight characterization and compensation of the optical properties of the EIT instrument," *Proc. SPIE*, 3765, 341–350 (1999).
[28] Clette, F., Hochedez, J. -F., Newmark, J. S., Moses, J. D., Auchère, F., Defise, J. -M., Delaboudinière, J.-P., "The Radiometric Calibration of the Extreme Ultraviolet Imaging Telescope," *The Radiometric Calibration of SOHO (ESA SR-002)*, Edited by A. Pauluhn, M.C.E. Huber and R. von Steiger, p.121 (2002).
[29] Shing, L., Stern, R. A., Catura, P., Morrison, M. D., Eaton, T., and Pool, P. J., "CCD development and characterization for the GOES N and O Solar X-ray Imager," *Proc. SPIE Vol. 3765, EUV, X-Ray, and Gamma-Ray Instrumentation for Astronomy X*, Oswald H. Siegmund; Kathryn A. Flanagan; Eds., pp. 299–309 (1999).
[30] Stern, R. A., Shing, L., Catura, P. R., Morrison, M. D., Duncan, D. W., Lemen, J. R., Eaton, T., Pool, P. J., Steward, R., Walton, D. M., and Smith, A. "Characterization of the flight CCD detectors for the GOES N and O solar x-ray imagers," *Proc. SPIE* 5171, pp. 77-88 (2004); doi: 10.1117/12.506346
[31] Baggett, S. M., Hill, R. J., Kimble, R. A., MacKenty, J. W., Waczynski, A., Bushouse, H. A., Boehm, N., Bond, H. E., Brown, T. M., Collins, N. R., Delo, G., Dressel, L., Foltz, R., Hartig, G., Hilbert, B., Kan, E., Kim-Quijano, J., Malumuth, E., Martel, A., McCullough, P., Petro, L., Robberto, M. and Wen, Y. "The Wide-field Camera 3 Detectors," *SPIE Proc.* Vol. 7021, 70211Q, (2008); doi: 10.1117/12.790056
[32] Bushouse, H., "WFC3 TV3 Testing: UVIS Science Monitor," *WFC3 Instrument Science Report* 2008-37 (2008)
[33] Collins *et al.*, "Wide Field Camera 3 CCD Quantum Efficiency Hysteresis: Characterization and Mitigation," *SPIE Proc.* 7439 (2009).
[34] Hoenk, M. E., Grunthaner, P. J., Grunthaner, F. J., Terhune, R. W., Fattahi, M., and Tseng, H.-F., "Growth of a delta-doped silicon layer by molecular beam epitaxy on a charge-coupled device for reflection-limited ultraviolet quantum efficiency," *Appl. Phys. Lett.* **61**: 1084 (1992).
[35] Nikzad, S., Hoenk, M. E., Grunthaner, P. J., Terhune, R. W., Grunthaner, F. J., Winzenread, R., Fattahi, M. M., and Tseng, H.-F.. "Delta-doped CCDs as stable, high-sensitivity, high-resolution UV imaging arrays," *Proc. SPIE 2217* (1994); doi: 10.1117/12.179949
[36] Jenkins, J. M., Borucki, W. J., Dunham, E. W., and McDonald, J. S., "High Precision Photometry with Back-Illuminated CCDs," *ASP Conf Ser* ,16-18 Oct. STScI (1996).
[37] Nikzad, S., Jones, T. J., Elliott, S. T., Cunningham, T. J., Deelman, P. W., Walker II, A. B. C., and Oluseyi, H. M., "Ultrastable and uniform EUV and UV detectors," *SPIE Proc.*, Vol. 4139, pp. 250-258, 2000.
[38] Headrick, R. L., Weir, B. E., Levi, A. F. J., Freer, B., Bevk, J., and Feldman, L. C., "Ordered monolayer structures of Boron in Si(111) and Si(100)," *J. Vac. Sci. Technol., A* 9(4): 2269-2272 (1991).
[39] Zhang, Z., Kulakov, M. A., Bullemer, B., Eisele, I. and Zotov, A. V., "Epitaxial growth of ultrathin Si caps on Si(100):B surface studied by scanning tunneling microscopy," *Appl. Phys. Lett.* **69**: 494 (1996).
[40] Weir, B. E., Feldman, L. C., Monroe, D. and Grossmann, H.-J., Headrick, R. L. and Hart, T. R., "Electrical characterization of an ultrahigh concentration boron delta-doping layer," *Appl. Phys. Lett.* 65(6): 737-739 (1994).
[41] Citrin, P. H., Muller, D. A., Gossmann, H.-J., Vanfleet, R. and Northrup, P. A., "Geometric Frustration of 2D Dopants in Silicon: Surpassing Electrical Saturation," *Phys. Rev. Lett*. 83: 3234 (1999).
[42] Citrin, P. H., Muller, D., Gossmann, H.-J., Vanfleet, R. and Northrup, P. A., "Breaking through the electrical saturation barrier: 2D- versus 3D-doping in n-type silicon," *Physica B* 273-274: 251-255 (1999).
[43] Hoenk, M. E., "Surface Passivation by Quantum Exclusion Using Multiple Layers," U.S. Patent 8,395,243, issued March 12, 2013; U.S. patent 9,024,344, continuation in part, issued May 5, 2015.
[44] Hoenk, M. E., Carver, A. G., Jones, T. J., Dickie, M., Nikzad, S., Sgro, J., and Tsur, S., "Superlattice-doped Imaging Detectors: Structure, Physics, and Performance," *Proceedings of the Scientific Detectors Workshop*, Florence, Italy, October 7-11 (2013)
[45] Hoenk, M. E., Nikzad, S., Carver, A. G., Jones, T. J., Hennessy, J., Jewell, A. D., Sgro, J., Tsur, S., McClish, M., and Farrell, R., "Superlattice-doped imaging detectors: progress and prospects," *SPIE Proc.* 9154, High Energy, Optical, and Infrared Detectors for Astronomy VI, 915413, Montreal, Canada (2014).
[46] Birner, S., "Modeling of semiconductor nanostructures and semiconductor–electrolyte interfaces," Ph.D. thesis, *Selected Topics of Semiconductor Physics and Technology*; v. 135; 126 p; ISBN 978-3-941650-35-0 (2011)

[47] Grunthaner, P. J., Grunthaner, F. J., Fathauer, R. W., Lin, T. L., Hecht, M. H., Bell, L. D., Kaiser, W. J., Schowengerdt, F. D., and Mazur, J. H., "Hydrogen-terminated silicon substrates for low temperature molecular beam epitaxy," *Thin Solid Films*, 183: 197-212 (1989).
[48] Hoenk, M. E., Hennessy, J., Jewell, A. D., Carver, A. G., Jones, T. J., Nikzad, S., McClish, M., Tsur, S., Meynants, G., and Sgro, J., "Superlattice-doped detectors for UV through gamma-ray imaging and spectroscopy," *Proceedings of the International Image Sensors Workshop*, Vaals, the Netherlands, June 8-11 (2015).
[49] Inoue, F., Jourdain, A., Peng, L., Phommahaxay, A., De Vos, J., Rebibis, K. J., Miller, A., Sleeckx, E., Beyne, E., and Uedono, A., "Influence of Si wafer thinning processes on (sub)surface defects," *Applied Surface Science* 404: 82–87 (2017).
[50] Mizushima, Y., Kim, Y., Nakamura, T., Sugie, R., Hashimoto, H., Uedono, A., Ohba, T., "Impact of back-grinding-induced damage on Si wafer thinning for three-dimensional integration," *Jpn. J. Appl. Phys.* **53**(5S2)**:** 05GE04, 2014; DOI: 10.7567/JJAP.53.05GE04
[51] Ogita, Y., Kobayashi, K., and Daio, H., "Photoconductivity characterization of silicon wafer mirror-polishing subsurface damage related to gate oxide integrity," *Journal of Crystal Growth* **210**: 36-39 (2000).
[52] Takizawa, R., Nakanishi, T., Honda, K., and Ohsawa, A., "Ultraclean Technique for Silicon Wafer Surfaces with HNO3-HF Systems," *Japanese Journal of Applied Physics*, 27(11): L2210-L2212 (1988).
[53] Correa, J. *et al.*, "On the Charge Collection Efficiency of the PERCIVAL Detector," *18th International Workshop on Radiation Imaging Detectors*, 3–7 July 2016, Barcelona, Spain.
[54] A.Khromova *et al.*, "Report on recent results of the PERCIVAL soft X-ray imager," *18th International Workshop on Radiation Imaging Detectors*, 3-7 July 2016, Barcelona, Spain (2016)
[55] A. Marras *et al.*, "Characterization of the Percival detector with soft X-rays," *J. Synchrotron Rad.* **28**: 131–145 (2021).
[56] Jewell, A. D., Looker, Q., Sanchez, M. O., Nikzad, S., and Hoenk, M. E., "Toward ultrafast, ultra-stable imaging arrays: Superlattice doping to enhance the performance of backside-illuminated 3D-hybridized silicon photodetectors," *Journal of Vacuum Science and Technology A* 38, 023203 (2020).
[57] Looker, Q., Aguirre, B. A., Hoenk, M. E., Jewell, A. D., Sanchez, M. O., and Tierney, B. D., "Superlattice-enhanced silicon soft X-ray and charged particle detectors with nanosecond time response," *Nuclear Instruments and Methods A*, 916, 148-153 (2019).
[58] Hoenk, M. E., Jones, T. J., Dickie, M. R., Greer, F., Cunningham, T. J., Blazejewski, E., and Nikzad, S., "Delta-doped back-illuminated CMOS imaging arrays: Progress and prospects," *SPIE Proc.* 7419, 74190T (2009).
[59] Nikzad, S., Hoenk, M. E., Greer, F., Jacquot, B., Monacos, S., Jones, T. J., Blacksberg, J., Hamden, E., Schiminovich, D., Martin, C., and Morrissey, P., "Delta-doped electron-multiplied CCD with absolute quantum efficiency over 50% in the near to far ultraviolet range for single photon counting applications," *Applied Optics*, **51**(3): 365-369 (2012).
[60] Greer, F., Hamden, E., Jacquot, B. C., Hoenk, M. E., Jones, T., Dickie, M., Monacos, S. P., and Nikzad, S. "Atomically Precise Surface Engineering of Silicon CCDs for Enhanced UV Quantum Efficiency", *Journal of Vacuum Science and Technology A* 01A103-1 (2013).
[61] Hennessy, J., Jewell, A. D., Hoenk, M. E., and Nikzad, S. "Metal–dielectric filters for solar–blind silicon ultraviolet detectors," *Applied Optics* 54(11): 3507-3512 (2015)
[62] Hamden, E. T., Jewell, A. D., Shapiro, C. A., Cheng, S. R., Goodsall, T. M., Hennessy, J., Hoenk, M. E., Jones, T., Gordon, S., Ong, H. R., Schiminovich, D., Martin, D. C., and Nikzad, S., "Charge-coupled devices detectors with high quantum efficiency at UV wavelengths," *J. Astron. Telesc. Instrum. Syst.* **2**(3), 036003 (2016).
[63] Nikzad, S., Hoenk, M. E., Jewell, A. D., Hennessy, J. J., Carver, A. G., Jones, T. J., Goodsall, T. M., Hamden, E. T., Suvarna, P., Bulmer, J., Shahedipour-Sandvik, F., Charbon, E., Padmanabhan, P., Hancock, B., and Bell, L. D., "Single Photon Counting UV Solar-Blind Detectors Using Silicon and III-Nitride Materials," *Sensors*, 16(6): 927, 2016.
[64] Nikzad, S., Jewell, A. D., Hoenk, M. E., Jones, T., Hennessy, J., Goodsall, T., Carver, A., Shapiro, C., Cheng, S. R., Hamden, E., Kyne, G., Martin, D. C., Schiminovich, D., Scowen, P., France, K., McCandliss, S., and Lupu, R. E., "High Efficiency UV/Optical/NIR Detectors for Large Aperture Telescopes and UV Explorer Missions: Development of and Field Observations with Delta-doped Arrays," *Journal of Astronomical Telescopes, Instruments, and Systems*, 3(3), 036002 (2017).
[65] Hennessy, J., Jewell, A. D., Hoenk, M. E., Hitlin, D., McClish, M., Carver, A. G., Jones, T. J., Morsy, A., Povinelli, M., Bell, L. D., and Nikzad, S. "Advanced imaging capabilities by incorporating plasmonics and metamaterials in detectors," *SPIE Proc.* 10639, 106391P (2018)

[66] Jewell, A. D., Hennessy, J., Jones, T., Cheng, S., Carver, A., Ardila, D., Shkolnik, E., Hoenk, M. E. and Nikzad, S., "Ultraviolet detectors for astrophysics missions: a case study with the star-planet activity research cubesat (SPARC)," *Proc. SPIE 10709, High Energy, Optical, and Infrared Detectors for Astronomy VIII*, 107090C (2018)
[67] Kyne, G., Hamden, E. T., Nikzad, S., Hoadley, K., Jewell, A., Jones, T., Hoenk, M. E., Cheng, S., Martin, D. C., Lingner, N., Schiminovich, D., Milliard, B., Grange, R., and Daigle, O., "Delta-doped electron-multiplying CCDs for FIREBall-2," *J. Astron. Telesc. Instrum. Syst.* 6(1), 011007 (2020); doi: 10.1117/1.JATIS.6.1.011007
[68] Hennessy, J. J., Jewell, A. D., Hoenk, M. E., and Nikzad, S. "Advances in detector-integrated filter coatings for the far ultraviolet," *SPIE Proc.* 11821, 118211A (2021).
[69] Heymes, J., Soman, M., Randall, G., Gottwald, A., Harris, A., Kelt, A., Moody, I., Meng, X., and Holland, A. D., "Comparison of Back-Thinned Detector Ultraviolet Quantum Efficiency for Two Commercially Available Passivation Treatments," *IEEE Transactions on Nuclear Science*, vol. 67, no. 8, pp. 1962-1967 (2020)